2024

3D Microtissue Model Of The Aged Ovarian Tumor Microenvironment

Peyton Clark
University of Alabama at Birmingham

3D MICROTISSUE MODEL OF THE AGED OVARIAN TUMOR MICROENVIRONMENT

by

PEYTON CLARK

MK SEWELL-LOFTIN, COMMITTEE CHAIR
REBECCA AREND
MYTHREYE KARTHIKEYAN

A THESIS

Submitted to the graduate faculty of The University of Alabama at Birmingham,
in partial fulfillment of the requirements for the degree of
Master of Science

BIRMINGHAM, ALABAMA

2024

3D MICROTISSUE MODEL OF THE AGED OVARIAN TUMOR MICROENVIRONMENT

PEYTON CLARK

BIOMEDICAL ENGINEERING

ABSTRACT

Ovarian cancer is the 5th leading cause of cancer deaths for women, primarily due to treatment resistant and/or recurrent disease. Most cases of ovarian cancer are not diagnosed until distant metastases have formed, which drastically reduces overall survival. The median age at diagnosis is 63 and most cases occur in patients who are peri- and post-menopausal. There is a critical gap between the clinical presentation of ovarian cancer and the preclinical models used to study the disease. Most preclinical *in vivo* investigations use mice who are between 6 and 12 weeks old, which corresponds to roughly a 20-year-old human. Therefore, there is a significant need to address the discrepancy between current *in vivo* and *in vitro* models to elucidate how the changes in the tumor microenvironment (TME) related to extracellular matrix (ECM) composition alter disease progression. The combination of age-related and cancer-related ECM remodeling poses a unique challenge to fully understanding the role of the ECM in ovarian cancer progression. In response to this challenge, we propose that a 3D TME model will allow for isolation and observation of the effects of ECM remodeling on ovarian cancer progression and serve as a model for ovarian cancer in aged patients. In this project, we fabricated matrices that correspond to different levels of maturity and both initial and advanced disease by altering hyaluronic acid and collagen content and evaluated changes in cell proliferation and SNAIL1, a protein implicated in cancer metastasis, expression in response to changes in the ECM. Generally, our results show

that SNAIL1 expression and proliferation increased with increasing HA and collagen content in the matrices. Additionally, we utilized a microfluidic device to analyze migration between matrices of different compositions. Our results suggest that matrix cues alone may not be sufficient to drive migration of ovarian cancer cells. Overall, we successfully fabricated a model of the ovarian TME that allows for precise control of the ECM to evaluate how changes affect proliferation of cells and other markers of disease progression.

Keywords: ovarian cancer, tumor microenvironment, mechanobiology, *in vitro* models, extracellular matrix

ACKNOWLEDGMENTS

I would like to acknowledge my committee members for their guidance and input on this project and for pushing me to be a better and stronger scientist.

I would like to thank my family, especially my parents who have supported me through every step of this process. I know that I would not be where I am today without their constant encouragement.

I would also like to thank my friends, especially Josh and Eirian, for always cheering me on in everything I do and making sure I have a place to go and decompress after a long week.

Finally, I would like to thank MK and the members of the Sewell-Loftin lab for their guidance through the confusing world of science and for not letting me quit when things got hard.

TABLE OF CONTENTS

Page

LIST OF TABLES

LIST OF FIGURES

Chapter 1

INTRODUCTION

High Grade Serous Ovarian Cancer

Ovarian cancer is the fifth leading cause of cancer deaths for women, with 12,740 predicted deaths in 2024, per the American Cancer Society[1]. The most recent average five-year survival rate in the United States is 51.2%[2]. It is estimated that 90% of ovarian cancers originate from transformed epithelial cells and are designated epithelial ovarian cancer (EOC)[3]. The EOC subtype consists of four histological subtypes that are defined by the morphology and tissue architecture of the tumor. The most aggressive and deadliest subtype of EOC is high grade serous ovarian carcinoma (HGSOC), which accounts for 70%-80% of all ovarian cancer deaths[3]. HGSOC tumors develop rapidly and at the time of diagnosis, over 50% of patients are found to have distant metastases, which corresponds to stage III and IV disease as defined by the Internation Federation of Gynecology and Obstetrics[2, 4]. This delayed diagnosis is due to a variety of factors, including the lack of defined symptoms, with many patients initially presenting with vague gastrointestinal symptoms such as abdominal pain, bloating, and nausea[3, 5] Most deaths due to ovarian cancer occur because of recurrent and/or treatment-resistant disease, with treatment resistance occurring in roughly 80-90% of patients initially diagnosed with advanced-stage disease and distant metasases[6].

The median age at diagnosis for ovarian cancer is 63, with the majority of cases occurring in patients who are over 50 years old[2]. The five-year survival rates decrease as the age at diagnosis increases with a rate of 74.7% for patient under 50 and a rate of only 34.1% for patients over 65[2]. Despite the decrease in survival as a patient ages, and the advanced age of most patients, the majority of *in vivo* laboratory studies performed utilize younger animals (age range) that have just reached sexual maturity, due to both time and cost constraints. This creates a discrepancy between the clinical presentation of ovarian cancer and how it is being studied in the labs. This discrepancy suggests a critical need for new research into improving and generating models that are more clinically relevant. In my project, the objective was to generate *in vitro* models that more closely mimic the clinical presentation of ovarian cancer by recapitulating the conditions of the aged ovary, specifically the extracellular matrix.

Ovarian Tumor Microenvironment

The tumor microenvironment (TME) consists of the matrix composition and organization, multiple different cell types, biomechanical forces in and near the tumor, and all the additional components in and around the tumor that drive progression . This includes fibrillar extracellular matrix proteins, fibroblasts, immune cells, vasculature and endothelial cells, and a variety of soluble and mechanical stimuli, such as shear fluid force, interstitial flow, compression, and tension[7]. A fundamental component of the TME is the extracellular matrix (ECM), which is made up of various fibrous proteins and proteoglycans that are secreted and remodeled by the stromal and tumor cells. The ECM serves as support and plays an important role in both healthy and cancerous tissues. The

ECM can alter a variety of cellular behaviors, including proliferation, migration, and metabolism[8-10]. Specifically ECM stiffness drives migration and morphology of EOC cells through mechanotransducive protein signaling, such as YAP, FAK, and the Rho-ROCK pathway[10]. Additionally, the ECM can alter proliferation, protein synthesis, and overall cell viability via mechanotransduction and altering cytoskeletal tension in the cell[8, 11]. In the case of ovarian cancer, two key components of the ECM are type I collagen and hyaluronic acid (HA).

Collagen in the Ovarian TME

Type I collagen is a highly abundant protein in both the healthy and cancerous ovarian ECM. It serves as a support protein and is important in tissue development and formation. Collagen I is a fibrillar collagen that is made of three α chains assembled into a triple helix[9]. In healthy tissue, collagen I is highly organized, and fibrils are parallel to the epithelial boundary. However, in cancerous tissues, collagen I fibrils are shorter, thicker, and tend to be perpendicular to the epithelium[9]. Increased collagen I content is associated with increased tissue stiffness, especially in cancerous tissues[8]. In ovarian cancer, increased collagen has been implicated in the promotion of migration and cell adhesion[9, 12]. Additionally, it has been shown that directional migration of some ovarian cancer cell lines is increased in the presence of collagen[13, 14]. Collagen is upregulated and more abundant in the ECM of multiple cancers and contributes to the epithelial-to-mesenchymal transition (EMT), a key step in tumor metastasis[15]. Cellular response to collagen is primarily mediated through integrins, specifically the β1 integrin and the ERK pathway, which is involved in cell adhesion and growth[16]. Additionally, collagen

increases intercellular Snail1 levels via DDR2 binding, leading to EMT and increased metastatic activity[17].

Hyaluronic Acid in the Ovarian TME

Hyaluronic acid (HA) is a glycosaminoglycan that has been implicated in a variety of cellular processes and its role in cancer progression has not yet been fully elucidated. HA is a polymer of alternating *N-acetyl-glucosamine* and glucuronic acid units and its size can reach 10MDa[18]. In normal tissue, HA plays an important role in tissue homeostasis, especially in maintaining tissue hydration and integrity[19]. In cancer, HA has been shown to modulate progression through interactions with cell surface receptors. Specifically, HA is involved in differentiation, proliferation, and cell migration, all key processes in tumor progression and metastasis[20]. The primary receptors for HA are CD44 and RHAMM, which impact cell proliferation, survival, and motility[19]. Additionally, HA is elevated in ovarian cancer stroma and is implicated in worsening disease progression[20]. In ovaries, it was found that HA content was 2-7 times higher in EOC tumors when compared to normal tissue[21]. It is known that different sizes of HA cause divergent cellular responses. Specifically, low molecular weight HA has been shown to induce an inflammatory response and can promote cell proliferation and migration[22].

Age-Associated Changes in Ovarian ECM

As a patient ages, changes to the ECM composition and organization occur that can alter cellular responses; such changes are important design considerations for developing *in vitro* models of advanced aged EOC patients. Specifically, ovaries from 14-17 month old mice, corresponding to roughly 47-56 year old humans, were stiffer as shown by a 2.5X increase in indention forces when compared to ovaries from 6-12 week old mice, corresponding to roughly 20 year old humans[23, 24]. Researchers determined that this change is primarily due to increases in collagen and decreases HA content in the ovaries. When the collagen in the ovaries from old mice was digested with collagenase, the stiffness of those ovaries resembled that of the ovaries from young mice[24]. These same researchers saw that the amount of HA in the stoma of the ovary decreases with age. This change is due to dysregulation in the enzymes that synthesize and degrade HA, specifically, hyaluronan synthase 3 (HAS3) and hyaluronidase 1 (HYAL1), which also causes changes in the molecular weight of HA present[24]. The changes in the ovarian ECM that occur with normal aging, combined with the changes that occur with cancer progression, represent a complex and dynamic environment and increases the difficulty in developing physiological relevant *in vitro* models for EOC studies.

3D *in vitro* TME Models

Many cancer studies, especially drug studies, are performed using two-dimensional cell culture where cells grow on tissue culture plastic in a monolayer, which fails to mimic the complicated native environment of cells and can result in the loss of

cell signaling pathways and changes in cell morphology[25]. An alternative to traditional 2-D cell culture is *in vivo* animal studies, but these are typically expensive and time consuming. *In vivo* models are also used as preclinical models and for the screening of potential therapies. The most common *in vivo* models of ovarian cancer utilize mice, which allow for observation of the effects of a full physiological environment. However, many murine models utilize immunocompromised animals in order to use human cancers, which fail to fully recapitulate the TME due to the lack of immune cells[26]. It is also virtually impossible to isolate cellular responses to controlled stimuli, such as small changes in the mechanical environment or precise delivery of soluble factors. To accurately model the physiological environment while maintaining the precise control over the surrounding environment necessary for tissue culture experiments, scientists have proposed a variety of 3-D culture methods. Some of the methods proposed involve suspending cells in hydrogels and synthetic scaffolds made of polymers such as polyethylene glycol (PEG) and poly(lactic-co-glycolic acid) (PLGA) to mimic the ECM and provide controllable mechanical stimuli[25]. However, these systems tend to be rather simple as they provide limited ability to control additional parameters such as interstitial flow. To address these concerns, more advanced 3-D systems have been developed based on microfluidic devices[25, 27-30]. These devices allow for complex systems to have various conditions, such as flow, matrix composition, and delivery of soluble factors, carefully controlled. They typically consist of tissue chambers that are constantly perfused by a network of microfluid channels[25, 27, 28, 30]. The advantages of microfluidic devices over other 3-D culture systems include more specific control of biochemical gradients, mechanical forces, and tissue interfaces. They are also less expensive, allow for a higher

volume of data to be analyzed at one time, and human cell models can be used[25, 31]. Another benefit of 3-D culture methods is the ability to modulate the TME to model the changes that may occur with disease progression and aging. Specifically, the composition of the ECM in these TME models can easily be altered to mimic ECM remodeling associated with various stages of disease. The current project focuses on optimizing a 3-D TME model based on a microfluidic platform to better understand how age and disease related changes in the ECM affect ovarian cancer progression.

Chapter 2

MATERIALS AND METHODS

Cell Culture

Human HGSOC model line SKOV3 cells with GFP reporter (SKOV3-GFP) were a generous gift of Dr. Mythreye Karthikeyan. SKOV3-GFP cells were maintained in RPMI-1640 (Corning, 10-040-CM) supplemented with 10% HI FBS (ThermoFisher Scientific, 10082-147) and 100U/ml penicillin streptomycin (Fisher Scientific, 15-140-122). Taxol-resistant SKOV3 (SKOV3.TR) cells were a generous gift of Dr. Rebecca Arend. SKOV3.TR cells were maintained in the same media as SKOV3-GFP cells but were treated with paclitaxel such that the concentration in the media was 0.5μM. All cells were incubated at 37°C and 5% CO_2 and received fresh media every other day. The cells were allowed to reach ~80% confluency before trypsinization and use in experiments. All cell lines used were immortalized.

3D Fibrin Ring Assay to Optimize Matrix Composition

Static TME models without interstitial flow were generated using a platform previously developed in our lab[28, 30]. These models allowed for the optimization of matrix composition before moving to more complex models. Briefly, 1cm rings with ID of 0.8cm made of polydimethylsiloxane (PDMS) were placed on glass coverslips, sterilized,

and put into 24-well plates. Cells were trypsinized and resuspended such that there would be 5k cells in each ring. Fibrin based gels were prepared by mixing fibrinogen (Sigma Aldrich, F8630-25G), thrombin (Sigma Aldrich, T4648-1KU, final concentration 3U/mL) with the addition of hyaluronic acid (Sigma Aldrich, 40583, 41897) and/or type I collagen (Fisher Scientific, NC1701927) as shown in **Table 1**. Additionally, 0.25U/ml aprotinin (Fisher Scientific, PI78432) was added to prevent fibrin degradation. Gel mixtures were prepared with a final total ECM protein concentration of 10mg/ml. The cells were suspended in the protein mixture and cast into the PDMS rings. Gels were then incubated for 30min at 37°C and 5% CO_2. Once polymerized, each gel was fed with 1mLof the appropriate media supplemented with 0.25U/ml aprotinin. Media was changed every 2 days and after 5 days, the gels were fixed for immunofluorescence analysis.

Microfluidic Device Studies

Our lab has previously developed a microfluidic device consisting of three independent microtissue chambers in series[28]. The chambers are connected with 20μm communication ports to allow transfer of nutrients and cell migration and chambers are fed independently through microfluidic lines (**Figure 1**). Cells were trypsinized and resuspended in fibrin-based gel mixtures with the addition of collagen and/or HA as shown in **Table 1**. Additionally, the membranes of SKOV3.TR cells were dyed using CellTracker™ Green CMFDA (ThermoFisher Scientific, C2925). Briefly, the cells were incubated for 30min in 10μM of the dye before being rinsed with media and resuspended at the desired concentration. The center chamber was loaded with 5k cells and blank cell-free gels with different ECM compositions were loaded into the side chambers. The

experimental setups are shown in **Table 2**. The devices were incubated for 30min at 37°C and 5% CO_2 to allow the gels to polymerize. Once polymerized the devices were fed into the center chamber, creating an interstitial flow outward to the side chambers. This outward flow washes away any soluble factors. The devices were fed daily with fresh media. Images were taken on day 0 and day 5 to track cell migration. Images of the devices were stitched using Pairwise Stitching and FIJI[32, 33]. After 5 days, the devices were fixed for immunofluorescence analysis.

Immunofluorescence Staining and Imaging

For immunofluorescence analysis, microtissues were fixed and stained for proliferation marker Ki67 and EMT protein SNAIL1. Additionally, SKOV3-GFP cells were stained with anti-GFP secondary to visualize cell shape. Briefly, rings were washed with 1X PBS three times and then fixed in 10% neutral buffered formalin for 30min. The rings were rinsed again in 1X PBS three times and then cell membranes were permeabilized using 1X PBS + 0.1% Tween-20 (PBST) for 30min. Then the microtissues were blocked in Abdil (PBST + 2% BSA) for 1h. Primary antibodies were diluted in Abdil and samples were incubated over night at 4°C on a rotator plate. The next day, the microtissues were washed 4X in PBST, each wash lasting 20min. Secondary antibodies were diluted in Abdil and samples were incubated overnight at 4°C on a rotator plate. Antibodies and concentrations are shown in **Table 3.** Finally, samples were washed for 20min in PBST twice, then incubated in DAPI (1:1000 in PBST) for 20min, before being washed a final time. Images were taken at 10X magnification using an inverted epifluorescence Olympus microscope (IX83) that captured 100μm stacks with a step-size

of 2μm for each sample. Images were processed using FIJI and the Extended Depth-of-Field plugin[33, 34]. To quantify expression levels, Ki67and SNAIL1 area was normalized to DAPI area.

Statistical Analysis

For all studies, data are reported as mean ± SEM with a minimum of 3 replicates. Data were first screened with Shapiro-Wilk test to evaluate normality. If all data in a set were normal, a one-factor ANOVA with post hoc Tukey HSD tests were performed. For any data sets that had at least one non-normal distribution, Kruskal-Wallis tests followed by post hoc Dunn's tests were performed. All statistical calculations were performed using the Real Statistics Resource package for Excel (https://real-statistics.com/). Statistical significance was considered at $p < 0.05$.

Table 1. Ratios of Fibrin(F):Collagen(Col):HA in matrix of 3D TME models

		No Collagen	Immature (Low Collagen)	Mature (High Collagen)
	No HA	10 (F)	9.5:0.5 (F:Col)	9:1 (F:Col)
Initial Disease	**Low HA**	9.5:0.5 (F:HA)	9.5:0.25:0.25 (F:Col:HA)	8:1.75:0.25 (F:Col:HA)
Advanced Disease	**High HA**	9:1 (F:HA)	8:0.25:1.75 (F:Col:HA)	8:1:1 (F:Col:HA)

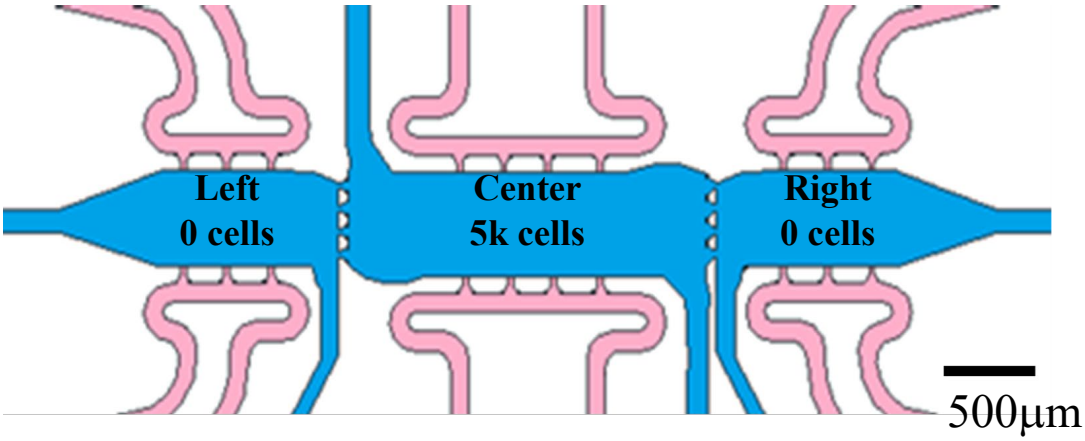

Figure 1. Schematic of Microfluidic Device. 3 tissue chambers (blue) connected in series fed by fluidic lines (pink). Loading conditions shown. Scale bar = 500µm. Note: Figure derived from "Micro-strains in the extracellular matrix induce angiogenesis" by MK Sewell-Loftin *et al.,* 2020 *Lab Chip*, *20*, p. 2776-2787[28].

Table 2. Device setups to study migration between matrices

Left **0 Cells**	**Center** **5k Cells**	**Right** **0 Cells**
Immature	Immature	Mature
Immature	Mature	Mature
Immature	no HA	Mature
Immature	no collagen	Mature
Immature	F only	Mature

Table 3. Antibodies and concentrations used for immunofluorescence analysis

Cells	Primary Antibodies	Secondary Antibodies
SKOV3-GFP	SNAIL polyclonal antibody (1:200, ThermoFisher Scientific, PA5-85493), Ki67 (8D5) Mouse mAb (1:2000, Cell Signaling Technology, 9449S)	Alexa Fluor 555 Donkey anti-MS (1:500, ThermoFisher Scientific, A31570), Alexa Fluor 647 Goat anti-Rb (1:500, ThermoFisher Scientific, A21236), Goat pAb to GFP (FITC) (1:1000, abcam, ab6662)
SKOV3.TR	SNAIL polyclonal antibody (1:200, ThermoFisher Scientific, PA5-85493), Ki67 (8D5) Mouse mAb (1:2000, Cell Signaling Technology, 9449S)	Alexa Fluor 555 Donkey anti-MS (1:500, ThermoFisher Scientific, A31570), Alexa Fluor 647 Goat anti-Rb (1:500, ThermoFisher Scientific, A21236)

Chapter 3

RESULTS

Collagen and HA content changes SKOV3 behavior in 3D cell culture

SKOV3-GFP cells were grown in 3D gels consisting of fibrin and differing concentrations of HA and collagen I for five days, then fixed and stained for Ki67 and SNAIL1 (**Figure 2A**). Our results indicate that SKOV3-GFP cells cultured with low amounts of 1MDa HA have increased SNAIL1 compared to systems with no HA or collagen (**Figure 2B**). For SKOV3-GFP cells cultured in high amounts of collagen, there is decreased SNAIL1 expression with the addition of high amounts of 10kDa HA (**Figure 2B**). Additionally, for SKOV3-GFP cells cultured in low amounts of collagen and 1MDa HA, an increase in collagen or an increase in HA seems to cause an increase in SNAIL1 expression (**Figure 2B**). In general, results show that increased collagen or HA in matrices may increase SNAIL1 expression in SKOV3-GFP cells. However, an increase in both collagen and HA does not further increase SNAIL1 expression. Furthermore, it appears that with high amounts of collagen, the addition of HA suppresses SNAIL1 expression.

Our results indicate that SKOV3-GFP cells cultured with high amounts of collagen or high amounts of HA show increased proliferation compared to cells cultured with no HA and low collagen (**Figure 2C**). Additionally, at high concentrations of HA, there is a trend that 1MDa HA decreases the proliferation of SKOV3-GFP cells compared

to 10kDA HA (**Figure 2C**). As expected, our results indicate that proliferation as measured by Ki67 staining is increased with increases in collagen and/or HA in the matrix.

Taxol-resistant SKOV3 cells have diminished response to change in matrix conditions

To investigate how changes in HA and collagen alter response in chemoresistant EOC cells, we studied the SKOV-3.tr line that is Taxol resistant compared to the parental SKOV-3 line. SKOV3.TR cells were grown in 3D gels consisting of fibrin and differing concentrations of HA and collagen I for five days, then fixed and stained for Ki67 and SNAIL1 (**Figure 3A**). Our studies show that SNAIL1 levels are lower in cells cultured in low concentrations of 10kDA HA compared with cells cultured in no collagen and no HA (**Figure 3B**). Additionally, those cells had lower SNAIL1 expression than cells grown with a high concentration of 1MDa HA (**Figure 3B**). The addition of a low concentration of collagen increased SNAIL1 expression for cells grown in low concentrations of 10kDA HA (**Figure 3B**). Additionally, increasing both the collagen and HA amounts increased SNAIL1 expression compared to cells grown in no collagen and a low concentration of 10kDA HA (**Figure 3B**). For proliferation, there was no significant change in the Ki-67 staining of SKOV3.TR cells grown in different gel compositions (**Figure 3C**). However, there is a trend that at high concentrations of HA, increasing the molecular weight from 10kDA to 1MDa decreases the proliferation. Overall, these results suggest that Taxol resistant SKOV3 cells display a diminished response to changes in

matrix conditions, but an increase in both HA and collagen content increases SNAIL1 expression.

Ovarian cancer cells did not migrate in microfluidic devices

As shown in **Table 2**, devices were set up to measure migration between matrices representing mature and immature ovarian TME as well as control matrices to determine the response to the addition of HA and collagen. SKOV3-GFP and SKOV3.TR cells were imaged on day 0 and day 7 (**Figure 4 and 5**) of incubation in the microfluidic device to monitor migration between the chambers. After 7 days, there was no migration from the center chambers into the side chambers of any of the devices.

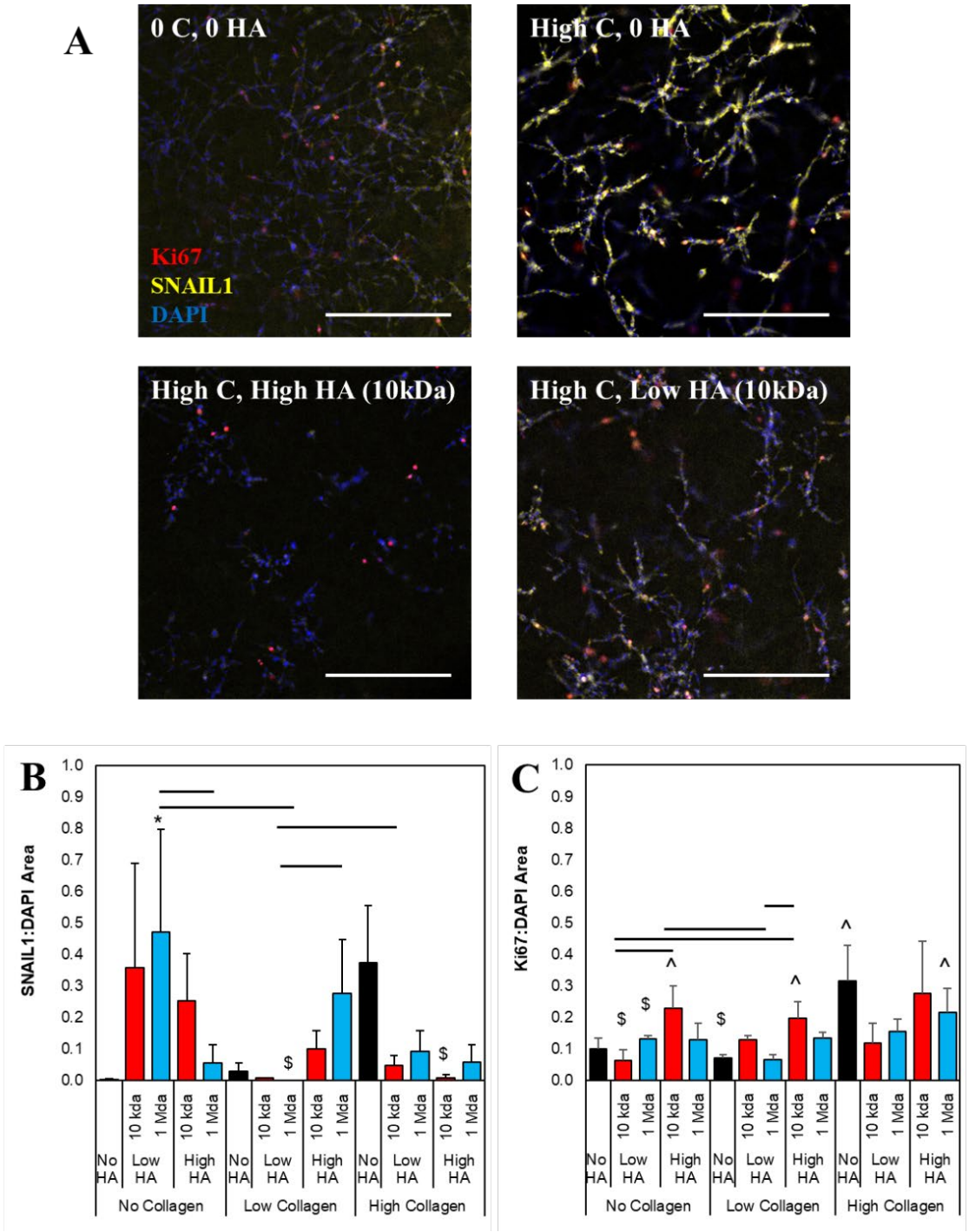

Figure 2. SNAIL1 and Ki67 expression in SKOV3-GFP cells in 3D ring assay. (A) Representative images of SKOV3-GFP microtissues stained for SNAIL1 (yellow) and Ki67 (red). Nuclei were stained with DAPI (blue). Matrix composition is shown, scale bar = 500μm. (**B**) Percent SNAIL1-Positive area and (**C**) Ki67-Positive area in microtissue models Averages ±SEM shown, n=3 per condition. * p< 0.05 vs no collagen, no HA, ^ p< 0.05 vs low collagen, no HA, $ p<0.05 vs high collagen, no HA, bar is p<0.05 between conditions.

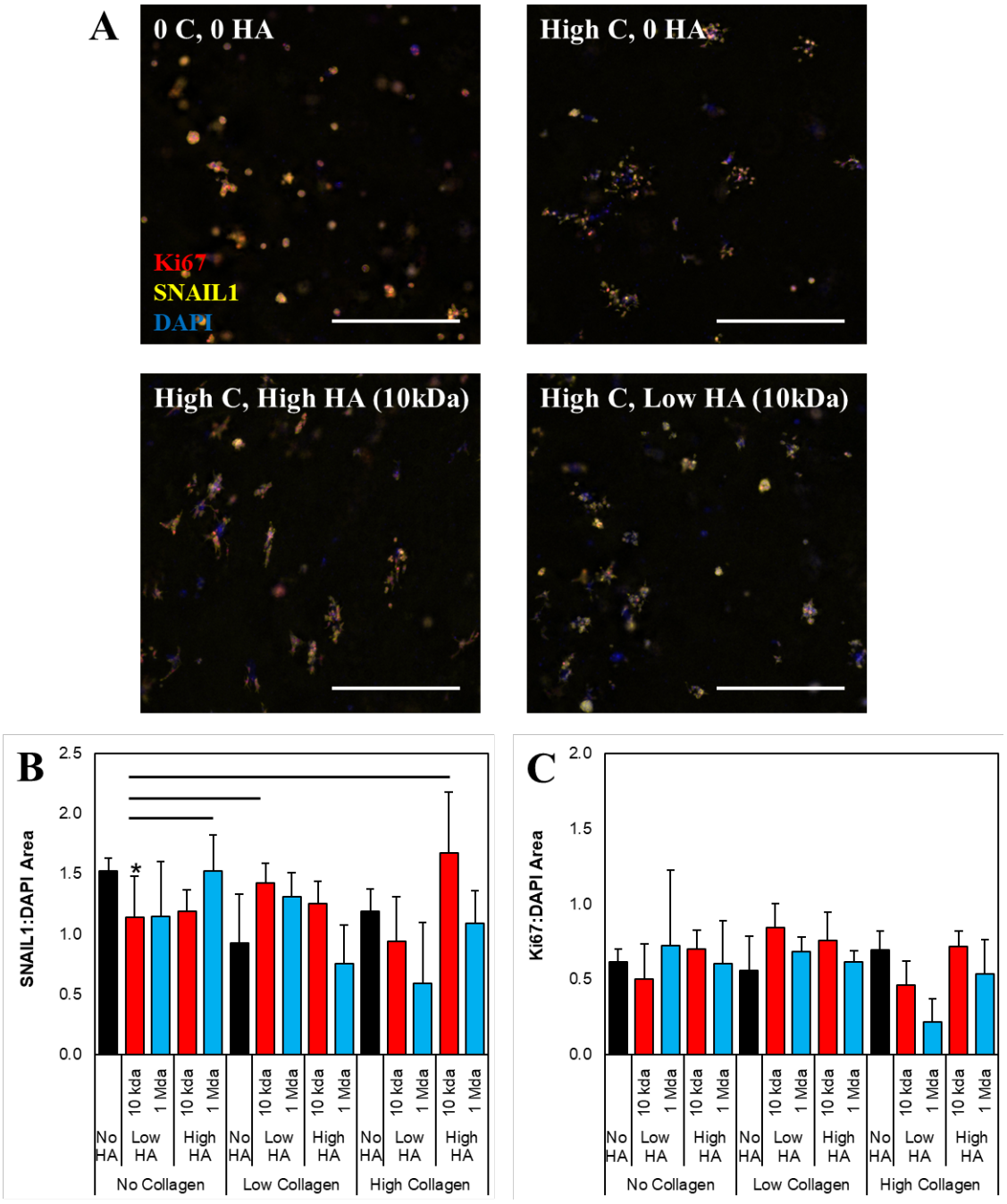

Figure 3. SNAIL1 and Ki67 expression in SKOV3.TR cells in 3D ring assay. (A) Representative images of SKOV3TR microtissues stained for SNAIL1 (yellow) and Ki67 (red). Nuclei were stained with DAPI (blue). Matrix composition is shown, scale bar = 500µm. (**B**) Percent SNAIL1-Positive area and (**C**) Ki67-Positive area in microtissue models Averages ±SEM shown, n=3 per condition. * $p < 0.05$ vs no collagen, no HA, bar is $p<0.05$ between conditions.

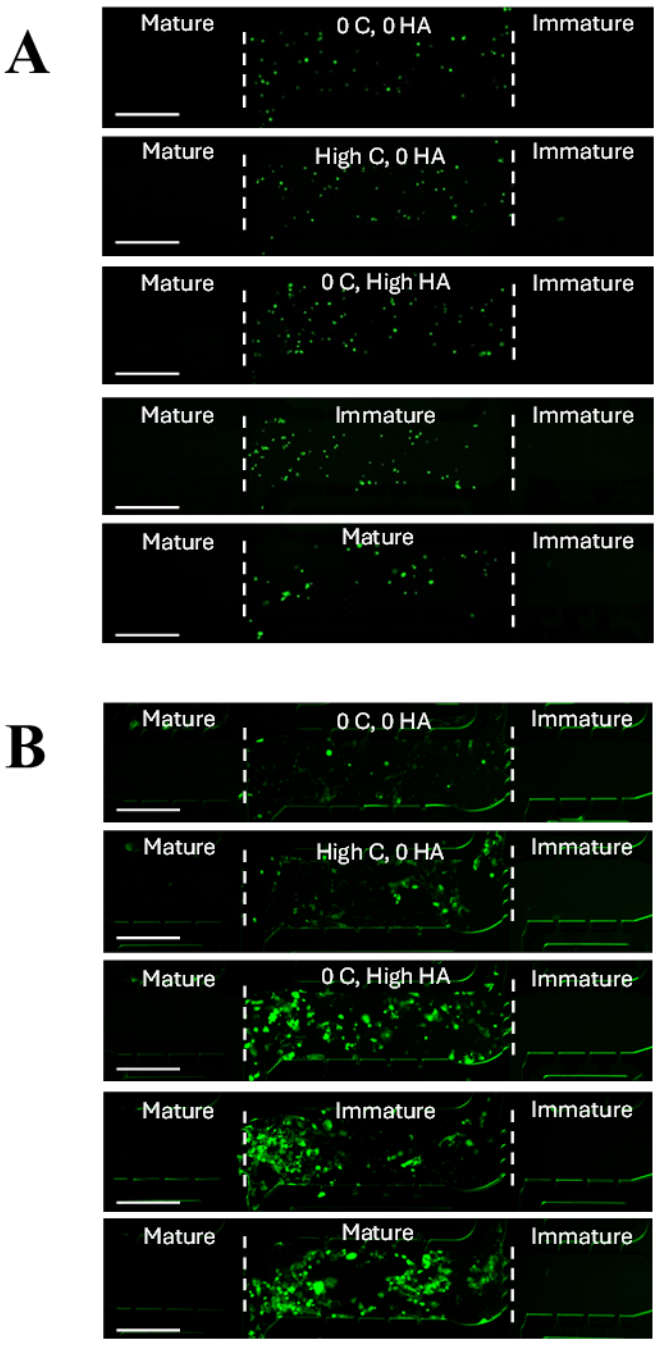

Figure 4. SKOV3-GFP cells in centipede devices. Representative images of SKOV3-GFP cell migration in microtissue model on day 0 (**A**) and day 7 (**B**). Tissue chamber boarders (white dashed lines) and treatments are shown. Scale bar = 100μm

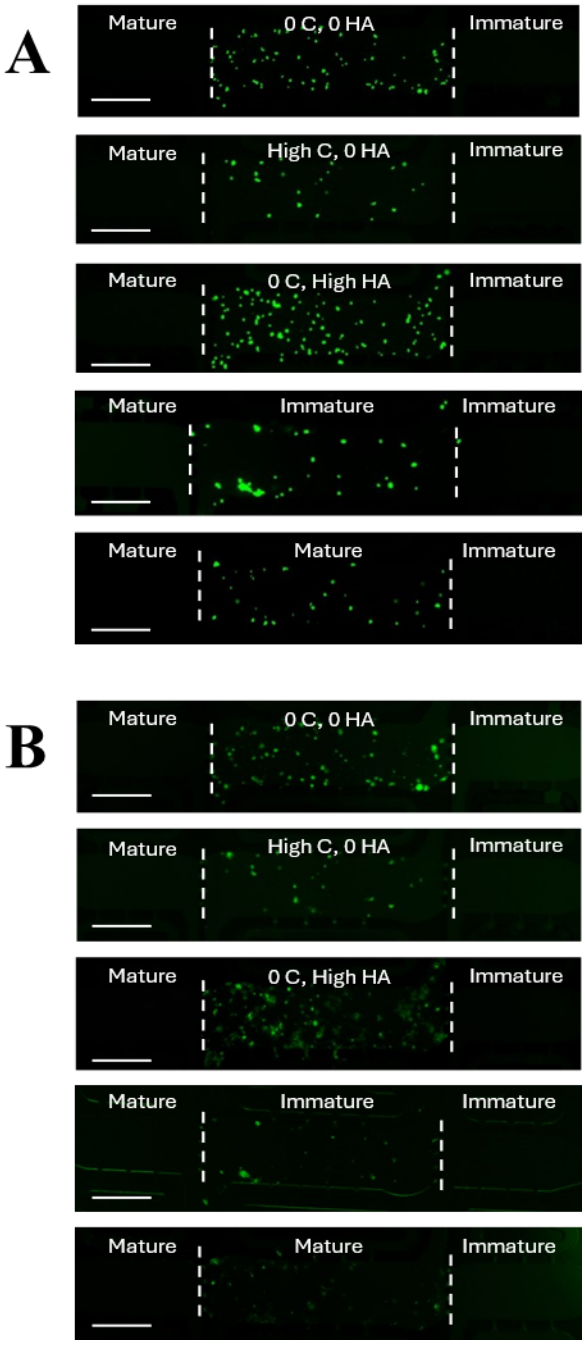

Figure 5. SKOV3.TR cells in centipede devices. Representative images of SKOV3.TR cell migration in microtissue model on day 0 (**A**) and day 7 (**B**). Cells were stained with CellTracker™ Green CMFDA for visualization. Tissue chamber boarders (white dashed lines) and treatments are shown. Scale bar = 100μm

Chapter 4

DISCUSSION

To model the effect aging has on cancer progression, we first generated *in vitro* models of the extracellular matrix of ovarian cancer. By changing the concentrations of collagen and HA in a fibrin-based gel, we generated matrices that roughly correspond to disease at various stages of severity and age. Specifically initial and advanced disease in both mature and immature ovaries (**Table 1**). The models, while fairly simple, allowed us to measure changes in cellular behavior in response to ECM changes associated with both age and cancer. Specifically, it has been shown that collagen content in the ovary increases as a patient ages and HA decreases[24]. The same researchers found that as collagen in the ovary increased, stiffness of the ovary also increased[24]. By altering the collagen and HA content in the matrices, we generated a model that facilitates the study of ovarian cancer in an aged ovary. Furthermore, our studies indicate that we can modulate HA and collagen content separately with a high degree of control to permit comparison between age-related matrix changes and tumor-associated matrix changes. This type of modeling is not possible in mouse ovarian cancer studies, where the mouse stroma is difficult to precisely alter.

In the models we generated, SNAIL1 expression tended to increase with HA in SKOV3. However, low molecular weight (10kDA) HA appeared to promote more SNAIL1 expression compared to high molecular weight (1MDa) HA at the same

concentrations (**Figure 2B**). This is in line with the literature that shows that low molecular weight HA triggers an inflammatory response and promotes migration and proliferation[22]. An increase in SNAIL1 suggests a more mesenchymal subtype and more migratory cells[17]. Furthermore, high concentrations of collagen without HA also increases SNAIL1 expression which is supported by other studies that suggest that collagen leads to EMT and is involved in the stabilization of SNAIL1[15-17]. Additionally, the decrease in SNAIL1 expression with the addition of HA in high collagen matrices, may be attributed to an increase in matrix density and steric hinderance which could prevent cell growth and migration. Unnikandam-Veettil, et. al, found that in collagen-HA composite matrices, the addition of HA decreased migration of breast cancer cells[35]. This decrease was attributed to a decrease in matrix pore size caused by the HA filling the pores in the collagen network[35].

In general, it appears that SKOV3.TR cells have higher levels of SNAIL1 expression than parental SKOV3 cells. This is potentially due to the selection for resistance causing the cells to be more aggressive. This is supported by the fact that drug resistant cells and drug resistant disease is more aggressive. Additionally, the presence of high amounts of collagen and high amounts of HA, corresponding to the aged ovary and advanced disease, increased SNAIL1 expression in SKOV3.TR cells (**Figure 3B**).

In SKOV3-GFP cells, HA promoted proliferation, however it appeared that low molecular weight HA caused higher levels of proliferation than high molecular weight HA (**Figure 2C**). This is supported by studies that have shown that low molecular weight promotes an inflammatory response and overall greater cell proliferation[22]. Furthermore, high levels of collagen also increased proliferation (**Figure 2C**), which is in line with the

literature that implicates collagen in integrin mediated proliferation[16]. However, the mechanism behind integrin mediated proliferation is beyond the scope of this project.

Overall SKOV3.TR cells have higher levels of proliferation compared to parental SKOV3 cells throughout all gel compositions. Even though not statistically significant, there is a trend that low molecular weight HA promoted higher levels of proliferation than high molecular weight HA (**Figure 3C**). The lower proliferation levels at high concentrations of collagen and HA may be due to matrix density inhibiting cell growth. This density may also inhibit cell migration, corresponding to lower SNAIL1 levels seen as well.

In microfluidic devices, there was no migration out of the center chambers for SKOV3-GFP cells and SKOV3.TR cells after 7 days (**Figure 4 and 5**). It is possible that the matrix composition of high collagen and 1MDa HA may be a physical barrier to migration. Further studies will involve increasing the cell number in the center chamber and studying migration over a longer time period. Additionally, low molecular weight HA, less HA, or less collagen may be used. Furthermore, the addition of soluble cues is possible in this model. This could involve the addition of stromal cells in the side chambers or using a growth factor as a potential chemoattractant.

Future Directions

In order to further characterize how age-associated changes in the ovarian TME affect cancer progression, the models introduced here need to be further developed and cellular response needs to be further characterized. Future studies will primarily involve

the use of the microfluidic device to simultaneously study cell migration, proliferation, and protein expression. Potential device setups include reducing the HA and collagen concentrations, increasing cell number in the center chamber, and the addition of relevant soluble factors from stromal cells. Additionally, other markers of disease progression such as vimentin and E-cadherin could be evaluated, with a decrease in E-cadherin and an increase in vimentin corresponding to a more mesenchymal phenotype and more aggressive cancer[36]. Furthermore, proteins associated with matrix remodeling and HA synthesis and degradation, specifically matrix metalloproteinases 2/9 and 7 (MMP2/MMP9, MMP7) and HAS3 and HYAL1, respectively[9]. Increased expression of MMP2/MMP9 and MMP7 would correspond to increase matrix remodeling by cancer cells and increased migration and metastatic potential[9]. Finally, these models could be used to determine how the ECM and changes in the TME modulate response of cancer cells to therapies.

Conclusion

Overall, this project has demonstrated that models of the aged ovarian TME can be easily generated and used to measure changes in disease progression in response to changes in the TME. These models address a critical gap between pre-clinical laboratory studies and the clinical presentation of ovarian cancer. Specifically, these models facilitate the study of ovarian cancer in a precisely controlled microenvironment in order to elucidate mechanisms and drivers of disease progression. Furthermore, these models can serve as a platform for initial testing of novel therapeutics in a clinically relevant environment. Generating accurate *in vitro* models of ovarian cancer is crucial to developing better treatments and a deeper understanding of the disease.

LIST OF REFERENCES

1. Siegel RL, Giaquinto AN, Jemal A. Cancer statistics, 2024. *CA: A Cancer Journal for Clinicians*. 2024;74(1):12-49. doi:https://doi.org/10.3322/caac.21820

2. SEER*Explorer: An interactive website for SEER cancer statistics. Surveillance Research Program, National Cancer Institute. https://seer.cancer.gov/statistics-network/explorer/

3. Lisio M-A, Fu L, Goyeneche A, Gao Z-h, Telleria C. High-Grade Serous Ovarian Cancer: Basic Sciences, Clinical and Therapeutic Standpoints. *International Journal of Molecular Sciences*. 2019;20(4):952.

4. Prat J. Staging classification for cancer of the ovary, fallopian tube, and peritoneum. *International Journal of Gynecology & Obstetrics*. 2014/01/01/ 2014;124(1):1-5. doi:https://doi.org/10.1016/j.ijgo.2013.10.001

5. Jayson GC, Kohn EC, Kitchener HC, Ledermann JA. Ovarian cancer. *The Lancet*. 2014;384(9951):1376-1388. doi:10.1016/S0140-6736(13)62146-7

6. Bowtell DD, Böhm S, Ahmed AA, et al. Rethinking ovarian cancer II: reducing mortality from high-grade serous ovarian cancer. *Nature Reviews Cancer*. 2015/11/01 2015;15(11):668-679. doi:10.1038/nrc4019

7. Bregenzer ME, Horst EN, Mehta P, Novak CM, Repetto T, Mehta G. The Role of Cancer Stem Cells and Mechanical Forces in Ovarian Cancer Metastasis. *Cancers*. 2019;11(7):1008.

8. Ge H, Tian M, Pei Q, Tan F, Pei H. Extracellular Matrix Stiffness: New Areas Affecting Cell Metabolism. Review. *Frontiers in Oncology*. 2021-February-24 2021;11doi:10.3389/fonc.2021.631991

9. Cho A, Howell VM, Colvin EK. The Extracellular Matrix in Epithelial Ovarian Cancer – A Piece of a Puzzle. Review. *Frontiers in Oncology*. 2015-November-02 2015;5doi:10.3389/fonc.2015.00245

10. McKenzie AJ, Hicks SR, Svec KV, Naughton H, Edmunds ZL, Howe AK. The mechanical microenvironment regulates ovarian cancer cell morphology, migration, and spheroid disaggregation. *Scientific Reports*. 2018/05/08 2018;8(1):7228. doi:10.1038/s41598-018-25589-0

11. Jaalouk DE, Lammerding J. Mechanotransduction gone awry. *Nature Reviews Molecular Cell Biology*. 2009/01/01 2009;10(1):63-73. doi:10.1038/nrm2597

12. Moser TL, Pizzo SV, Bafetti LM, Fishman DA, Stack MS. Evidence for preferential adhesion of ovarian epithelial carcinoma cells to type I collagen mediated by the αA2β1 integrin. *International Journal of Cancer*. 1996;67(5):695-701. doi:https://doi.org/10.1002/(SICI)1097-0215(19960904)67:5<695::AID-IJC18>3.0.CO;2-4

13. Flate E, Stalvey JRD. Motility of select ovarian cancer cell lines: Effect of extra-cellular matrix proteins and the involvement of PAK2. *Int J Oncol*. 2014/10/01 2014;45(4):1401-1411. doi:10.3892/ijo.2014.2553

14. Shen Y, Shen R, Ge L, Zhu Q, Li F. Fibrillar Type I Collagen Matrices Enhance Metastasis/Invasion of Ovarian Epithelial Cancer Via β1 Integrin and PTEN Signals. *International Journal of Gynecologic Cancer*. 2012;22(8):1316-1324. doi:10.1097/IGC.0b013e318263ef34

15. Shi R, Zhang Z, Zhu A, et al. Targeting type I collagen for cancer treatment. *International Journal of Cancer*. 2022;151(5):665-683. doi:https://doi.org/10.1002/ijc.33985

16. Ahmed N, Riley C, Rice G, Quinn M. Role of Integrin Receptors for Fibronectin, Collagen and Laminin in the Regulation of Ovarian Carcinoma Functions in Response to a Matrix Microenvironment. *Clinical & Experimental Metastasis*. 2005/09/01 2005;22(5):391-402. doi:10.1007/s10585-005-1262-y

17. Zhang K, Corsa CA, Ponik SM, et al. The collagen receptor discoidin domain receptor 2 stabilizes SNAIL1 to facilitate breast cancer metastasis. *Nature Cell Biology*. 2013/06/01 2013;15(6):677-687. doi:10.1038/ncb2743

18. Tammi RH, Kultti A, Kosma V-M, Pirinen R, Auvinen P, Tammi MI. Hyaluronan in human tumors: Pathobiological and prognostic messages from cell-associated and stromal hyaluronan. *Seminars in Cancer Biology*. 2008/08/01/ 2008;18(4):288-295. doi:https://doi.org/10.1016/j.semcancer.2008.03.005

19. Toole BP. Hyaluronan: from extracellular glue to pericellular cue. *Nature Reviews Cancer*. 2004/07/01 2004;4(7):528-539. doi:10.1038/nrc1391

20. Anttila MA, Tammi RH, Tammi MI, Syrjänen KJ, Saarikoski SV, Kosma V-M. High Levels of Stromal Hyaluronan Predict Poor Disease Outcome in Epithelial Ovarian Cancer1. *Cancer Research*. 2000;60(1):150-155.

21. Hiltunen ELJ, Anttila M, Kultti A, et al. Elevated Hyaluronan Concentration without Hyaluronidase Activation in Malignant Epithelial Ovarian Tumors1. *Cancer Research*. 2002;62(22):6410-6413.

22. Turley EA, Noble PW, Bourguignon LYW. Signaling Properties of Hyaluronan Receptors *. *Journal of Biological Chemistry*. 2002;277(7):4589-4592. doi:10.1074/jbc.R100038200

23. Hagan C. When are mice considered old? . 2017. https://www.jax.org/news-and-insights/jax-blog/2017/November/when-are-mice-considered-old#

24. Amargant F, Manuel SL, Tu Q, et al. Ovarian stiffness increases with age in the mammalian ovary and depends on collagen and hyaluronan matrices. *Aging Cell*. 2020;19(11):e13259. doi:https://doi.org/10.1111/acel.13259

25. Rodrigues J, Heinrich MA, Teixeira LM, Prakash J. 3D In Vitro Model (R)evolution: Unveiling Tumor–Stroma Interactions. *Trends in Cancer*. 2021/03/01/ 2021;7(3):249-264. doi:https://doi.org/10.1016/j.trecan.2020.10.009

26. Kramer M, Criswell A, Sewell-Loftin MK. Biomaterial considerations for ovarian cancer models. Review. *Frontiers in Materials*. 2023-August-03 2023;10doi:10.3389/fmats.2023.1223276

27. Ibrahim LI, Hajal C, Offeddu GS, Gillrie MR, Kamm RD. Omentum-on-a-chip: A multicellular, vascularized microfluidic model of the human peritoneum for the study of ovarian cancer metastases. *Biomaterials*. 2022/09/01/ 2022;288:121728. doi:https://doi.org/10.1016/j.biomaterials.2022.121728

28. Sewell-Loftin MK, Katz JB, George SC, Longmore GD. Micro-strains in the extracellular matrix induce angiogenesis. 10.1039/D0LC00145G. *Lab on a Chip*. 2020;20(15):2776-2787. doi:10.1039/D0LC00145G

29. Loessner D, Stok KS, Lutolf MP, Hutmacher DW, Clements JA, Rizzi SC. Bioengineered 3D platform to explore cell–ECM interactions and drug resistance of epithelial ovarian cancer cells. *Biomaterials*. 2010/11/01/ 2010;31(32):8494-8506. doi:https://doi.org/10.1016/j.biomaterials.2010.07.064

30. Sewell-Loftin MK, Bayer SVH, Crist E, et al. Cancer-associated fibroblasts support vascular growth through mechanical force. *Scientific Reports*. 2017/10/03 2017;7(1):12574. doi:10.1038/s41598-017-13006-x

31. Ahmed MAM, Nagelkerke A. Current developments in modelling the tumour microenvironment in vitro: Incorporation of biochemical and physical gradients. *Organs-on-a-Chip*. 2021/11/01/ 2021;3:100012. doi:https://doi.org/10.1016/j.ooc.2021.100012

32. Preibisch S, Saalfeld S, Tomancak P. Globally optimal stitching of tiled 3D microscopic image acquisitions. *Bioinformatics*. 2009;25(11):1463-1465. doi:10.1093/bioinformatics/btp184

33. Schindelin J, Arganda-Carreras I, Frise E, et al. Fiji: an open-source platform for biological-image analysis. *Nature Methods*. 2012/07/01 2012;9(7):676-682. doi:10.1038/nmeth.2019

34. Forster B, Van De Ville D, Berent J, Sage D, Unser M. Complex wavelets for extended depth-of-field: A new method for the fusion of multichannel microscopy images. *Microscopy Research and Technique*. 2004;65(1-2):33-42. doi:https://doi.org/10.1002/jemt.20092

35. Unnikandam Veettil SR, Hwang D, Correia J, Bartlett MD, Schneider IC. Cancer cell migration in collagen-hyaluronan composite extracellular matrices. *Acta Biomaterialia*. 2021/08/01/ 2021;130:183-198. doi:https://doi.org/10.1016/j.actbio.2021.06.009

36. Wells A, Yates C, Shepard CR. E-cadherin as an indicator of mesenchymal to epithelial reverting transitions during the metastatic seeding of disseminated carcinomas. *Clin Exp Metastasis*. 2008;25(6):621-8. doi:10.1007/s10585-008-9167-1

37. Kurman RJ, Shih Ie M. The Dualistic Model of Ovarian Carcinogenesis: Revisited, Revised, and Expanded. *Am J Pathol*. Apr 2016;186(4):733-47. doi:10.1016/j.ajpath.2015.11.011

38. Lengyel E. Ovarian cancer development and metastasis. *Am J Pathol*. Sep 2010;177(3):1053-64. doi:10.2353/ajpath.2010.100105

39. Do T-V, Kubba LA, Du H, Sturgis CD, Woodruff TK. Transforming Growth Factor-β1, Transforming Growth Factor-β2, and Transforming Growth Factor-β3 Enhance Ovarian Cancer Metastatic Potential by Inducing a Smad3-Dependent Epithelial-to-Mesenchymal Transition. *Molecular Cancer Research*. 2008;6(5):695-705. doi:10.1158/1541-7786.Mcr-07-0294

40. Walton J, Blagih J, Ennis D, et al. CRISPR/Cas9-Mediated Trp53 and Brca2 Knockout to Generate Improved Murine Models of Ovarian High-Grade Serous Carcinoma. *Cancer Res*. Oct 15 2016;76(20):6118-6129. doi:10.1158/0008-5472.Can-16-1272

APPENDIX

3D Microtissue Model for Quantifying Cancer Cell Migration and Directionality in Response to Soluble Factor

Introduction

High grade serous ovarian carcinoma (HGSOC) accounts for 90% of deaths as a result of ovarian cancer[37]. The process of metastasis of HGSOC begins with an epithelial-to-mesenchymal transition (EMT), which promotes the migration of the cancer cells and decreases intercellular attachment[38]. In order to induce migration, we utilized Transforming Growth Factor β (TGF-β1), which has been shown to promote EMT in ovarian cancer[39]. The objective of our study was to utilize a three-chamber microfluidic device and live cell microscopy to study the cellular response of ID8 cells to TGF-β1 over time as a model of metastatic migration behaviors and to show the model can be used to characterize migration.

Materials and Methods

ID8 cells with a *Trp53* $^{-/-}$ deletion are an established murine model of high grade serous ovarian cancer that allows for investigation of the tumor microenvironment[40]. ID8 cells were seeded into the center chamber of a three-chamber microfluidic device. Each chamber is an independent microtissue region, connected with 20μm wide communication ports to allow for cells to move between chambers (**Figure S1A**). The cells were suspended in a 9:1 fibrin-collagen gel, to mimic the natural tumor environment. The side chambers were filled with blank gels. For 3 days, systems were cultured so no diffusive flow occurred between adjacent chambers. Prior to imaging, the left chambers of all devices were treated with TGF-β1 (10 ng/ml) and an inward flow pattern (Left or Right chamber to Center chamber) was established. The devices were then imaged over either a 3-hour period or an 18-hour period with images taken every 5

minutes or 30 minutes respectively. After 24 hours of treatment, cell migration was quantified using the Chemotaxis and Migration Tool V2.0 (https://ibidi.com/chemotaxis-analysis/171-chemotaxis-and-migration-tool.html).

Results

The results show that in order to trigger a significant change in cellular behavior, a prolonged exposure to TGF-β1 is required (**Figure S1B**). In the short time frame, TGF-β1 stimulation alone slightly increases migration distance. To further characterize cell migration, we generated histograms displaying migration angles for individual cells, with 180° indicating movement towards the TGF-β1 in the Left chamber (**Figure S1C**). Interquartile ranges (IQRs), representing the middle 50% of all migration angle data, were quantified. Adding TGF-β1 reduces the IQR, indicating that the growth factor causes a more directed migration at both time points.

Conclusions

We have successfully developed a model of ovarian cancer migration with the ability to control matrix properties and delivery of growth factors. Further studies will investigate how mechanical properties of tumor and stromal compartments alter metastatic potential.

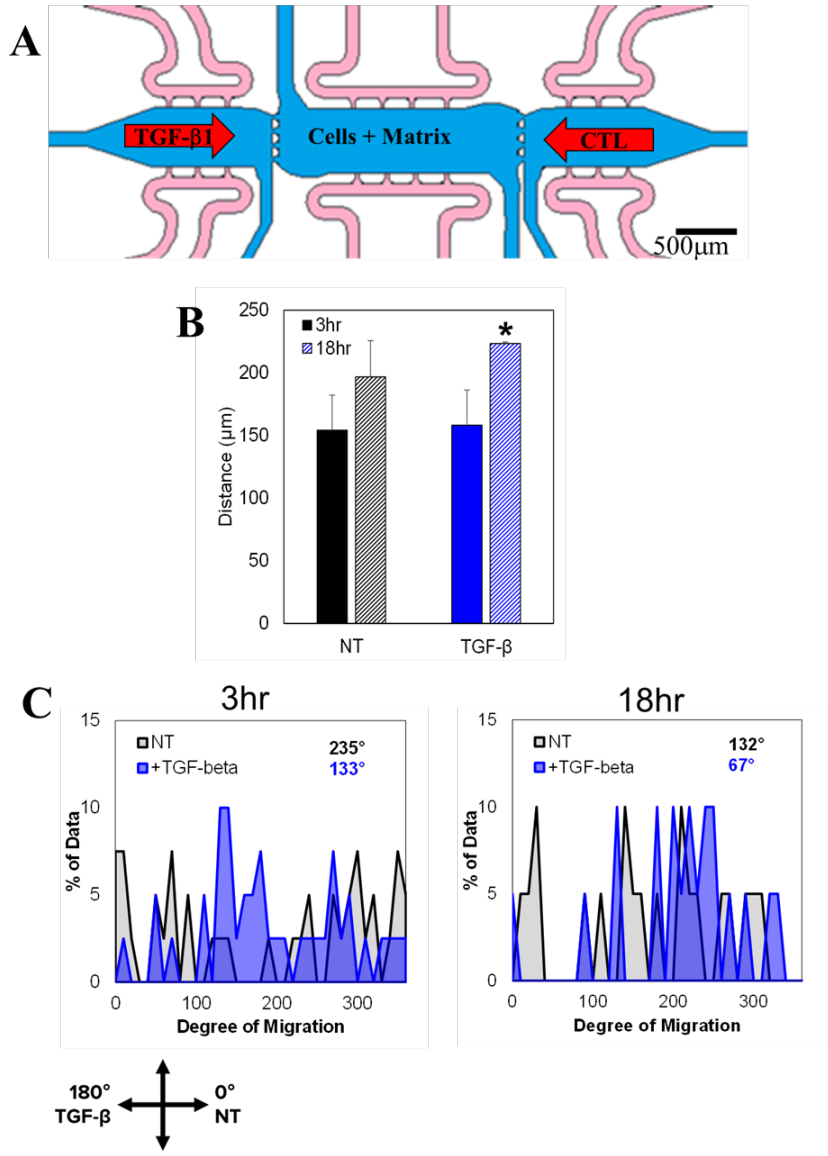

Figure S1. **Prolonged exposure to TGF-β1 increases migration distance and directionality.** (**A**) Microtissue model used to migration studies. Tissue chambers (blue), fluid lines (pink), and treatments are shown. Scale bar = 500µm. (**B**) Distance traveled by ID8p53 cells in the microtissue model. Averages ± SEM shown. N = 2-4 devices. * $p < 0.05$ vs. 3hr NT. (**C**) Histograms showing angles of migration for cells in microtissue models. 180° represents migration towards the Left chamber, or source of TGF-b1. Inset numbers are interquartile ranges (middle 50%) of all measured events, n=20-40 cells.